Z. Phys. B 100, 477–488 (1996)

ZEITSCHRIFT
FÜR PHYSIK B

Oblique rolls in nematic liquid crystals driven by stochastic fields: one-dimensional theory including the flexoeffect and three-dimensional theory

Adrian Lange[1], **Reinhard Müller**[2], **Ulrich Behn**[2]

[1] Theoretical Physics, University of Oxford, 1 Keble Road, Oxford OX1 3NP, UK
[2] Institut Theoretische Physik, Universität Leipzig, Augustusplatz 10, D-04109 Leipzig, Germany
(e-mail: phyub@hpwork24.physik.uni-leipzig.de)

Received: 14 May 1993 / Revised version: 12 June 1995

Abstract. The formation of oblique rolls in nematic liquid crystals driven by dichotomous stochastic fields is investigated in the frame of a one-dimensional linear theory including the flexoeffect, and in the frame of a three-dimensional linear theory with free boundary conditions. In the first model the threshold for the stability of the first moments is calculated and the angle of the oblique rolls is determined by mode selection. It is shown that in certain parameter ranges oblique rolls have lower thresholds than normal rolls. As for deterministic excitation, with increasing flexoeffect the formation of oblique rolls is favoured. It is observed that at full strength the flexoeffect alone is able to trigger the formation of rolls. In the three-dimensional model the threshold for the stability of the first moments is calculated again and the two wave numbers which give the angle of the oblique rolls are determined by mode selection. The appearance of oblique rolls is studied for different parameters of the driving stochastic field. The results are compared with those of the one-dimensional model without the flexoeffect.

PACS: 02.50. − r; 05.40. + j; 47.20. − k; 47.65. + a

1. Introduction

Electrohydrodynamic instabilities in nematic liquid crystals have recently been studied both experimentally and theoretically for deterministic as well as for stochastic excitation [1–16]. For the superposition of a constant and a dichotomous stochastic field [14–16] a linear analysis testing the stability against normal rolls can qualitatively explain (i) the discontinuous behaviour of the threshold above a critical strength of the noise, (ii) the change from discontinuous to continuous behaviour of the threshold with increasing correlation time of the noise, and (iii) the change from stabilizing to destabilizing effect of the noise if its correlation time becomes comparable to the relaxation time of the space charge.

Quantitatively, however, the strength of the stochastic voltage, above which the discontinuous behaviour occurs, is about a factor three too large if one compares the experimental data with the thresholds for the stability of the first moments. Since we would restrict ourself to a linear theory to extend the benefits of a previous developed method [15] the options for a better qualitative and quantitative agreement between theory and experiment are limited.

One option is to test the new patterns of oblique rolls and rhombic cells in the context of *stochastic* excitation. Oblique rolls have already been tested in deterministic square wave [17] and sinusoidal excitation [12, 18–20]. Rhombic cells can be represented as a superposition of oblique rolls with angles $+\delta$ and $-\delta$. Since in a *linearized* theory the superposition principle holds, oblique rolls and rhombic cells have the same threshold. Only a nonlinear theory could discriminate the two patterns. We therefore use the term oblique rolls as a synonym for both patterns. We test their stability against different types of excitation in a one-dimensional and in a three-dimensional linearized theory. In the three-dimensional model the patterns were described by a *general* ansatz which differs from the special ones used for three-dimensional calculations in [12, 21]. A three-dimensional model is advantageous since it allows the determination of two wave numbers of the patterns by mode selection. In contrast, there is no mode selection for the wave numbers in a one-dimensional model, and only one wave number can be determined in such a way in a two-dimensional model. For all our calculations we assume a supercritical bifurcation for the first instability, to which we are limited due to the linearized theory.

Alternatively the flexoeffect may be included in the calculations of the thresholds [17, 19–24]. The flexoeffect leads to a flexoelectric polarisation, $\boldsymbol{P}_{FL} = e_1 \hat{n} \operatorname{div} \hat{n} - e_3 \hat{n} \times \operatorname{rot} \hat{n}$, induced by splay- or bend-distortions [25, 26] of the liquid crystal (e_1 and e_3 are the flexoelectric coefficients). Both, free energy density and displacement are modified, $F \to F - \boldsymbol{E}\boldsymbol{P}_{FL}$, and $\boldsymbol{D} \to \boldsymbol{D} + 4\pi \boldsymbol{P}_{FL}$, which produces an additional term $\boldsymbol{\Gamma}_{FL}$ in the torque

balance equation and a contribution to the charge density, respectively.

The main aim of this paper is to consider these two new aspects in electrohydrodynamic instabilities with *multiplicative* noise. Additionally we obtained new interesting results for non-stochastic excitation, especially for DC excitation which has become the focus of great interest recently [27, 28].

The rest of the paper is organized as follows: In Sect. 2 we present the linearized electrohydrodynamic equations for the one-dimensional theory including the flexoeffect. We calculate the thresholds for a constant electric field (Subsect. 2.1) as a function of both the anisotropy of the conductivity $\sigma_\parallel/\sigma_\perp$ and the strength of the flexoeffect. In Subsect. 2.2 we analyze the stability of the first moments for pure stochastic excitation. Results are presented for a superposition of a constant and a stochastic electric field (Subsect. 2.3) which depend on the order of the correlation time of the noise compared with the characteristic time of the system. In Sect. 3 the full three-dimensional linear theory with free boundary conditions neglecting the flexoeffect is formulated. We calculate the thresholds for the three different types of excitation: For a constant field (Subsect. 3.1), for a pure stochastic field (Subsect. 3.2), and finally for a superposition of both (Subsect. 3.3). In Sect. 4 we give a conclusion and discuss the perspectives of nonlinear models.

2. One-dimensional theory including the flexoeffect

We consider a quasi one-dimensional linear theory including the flexoeffect [22–24] which tests the stability of the homogeneous nematic state against the formation of oblique rolls. In a sandwich cell of thickness d (we choose 100 μm) the initially unperturbed director $\hat{n}$ is oriented parallel to the electrode plates which lie in the xy-plane. As shown in Fig. 1 the disturbed director $\hat{n}$ includes the angle ϑ with the xz-plane, and the angle φ with the xy-plane. In the coordinate system $\xi\eta z$ rotated around the z-axis by the angle δ with respect to the xyz-system, the variables are the charge density q, the angle ϑ, and $\psi = \partial_\xi \varphi$. These and the other *internal* quantities, the hydrodynamic velocity in z-direction v_z and the electric field in ξ-direction E_ξ, depend on ξ and t, whereas the *external* driving electric field E_t depends on z and t. Throughout this paper we consider E_t as spatially homogeneous between the two electrodes.

The electrohydrodynamic equations for a nematic liquid crystal are the torque balance equation (dynamic equation for the director), the Navier-Stokes equation, the Maxwell equation for the displacement, and the continuity equation (see [29], equations (II,6), (II,9), (II,13), and (II,19) or [30], equations (8, 14, 26, 29)). The resulting five non-trivial partial differential equations for $\delta \geq 0$ allow the substitution of $\partial_{\xi\xi} v_z$ and $\partial_\xi E_\xi$ (arising during the derivation) without any approximation.

The linearized electrohydrodynamic equations describing the stability against an oblique roll pattern characterized by a wave number k_ξ and the angle δ read

$$\dot{q} + \frac{1}{T_q} q + \sigma_H E_t \psi + \frac{q_\vartheta}{T_q} \vartheta = 0, \tag{1}$$

$$\dot{\psi} + a E_t q + \frac{1}{T_\psi} \psi + b E_t \vartheta = 0, \tag{2}$$

$$\dot{\vartheta} + \frac{e_q}{\gamma_1} q + \frac{e_\psi}{\gamma_1} E_t \psi + \frac{1}{T_\vartheta} \vartheta = 0. \tag{3}$$

The structure of (1–3) is equivalent to deterministic square wave excitation (confer [17], equations (1–3)). $1/T_\psi$ depends on the square of the driving field E_t as well as the wave number k_ξ and the angle δ of the oblique rolls, as given in Appendix A. The other coefficients depend on the material constants of the nematic liquid crystal and δ, where q_ϑ, b, and T_ϑ depend additionally on k_ξ (see appendix A).

A recent review of the experimental measurements of the flexoelectric coefficients discussed the errors for the values of $(e_1 - e_3)$ and $(e_1 + e_3)$ ([31] and references therein). We therefore introduce two scaling factors which both take either the value zero (no flexoeffect) or values according to the estimated errors of 10% for $(e_1 - e_3)$ [31] and of 30% for $(e_1 + e_3)$ [32]. $\lambda_- \in \{0; [0.9, 1.1]\}$ scales the standard value $(e_1 - e_3) = 4 \cdot 10^{-12} \mathrm{Cm}^{-1}$ [33] and $\lambda_+ \in \{0; [0.7, 1.3]\}$ scales the standard value $(e_1 + e_3) = -2.3 \cdot 10^{-12} \mathrm{Cm}^{-1}$ [32], respectively.

The homogeneous state becomes unstable if the linear solutions of equations (1–3) grow exponentially. This defines a threshold of the driving field which depends on material constants and on test mode parameters. Usually the structure which gives the minimal threshold is selected. In one-dimensional theories however, one sets $k_\xi = \pi/d$ [14-16, 29, 30]. (Since the threshold is proportional to k_ξ the selected wavelength would tend toward infinity, in contrast to experience.) Only the oblique roll angle δ is determined by mode selection.

For excitation with a stochastic electric field, $E_t = E_1 + E_t^{DMP}$, where E_t^{DMP} is a dichotomous Markovian process jumping with mean frequency α between $\pm E$, one can derive closed equations describing the stability of moments [14–16]. To investigate the stability of the first moments we write (1–3) in matrix form, $\dot{\boldsymbol{z}} + (\mathbf{A} + \mathbf{B} E_t^{DMP}) \boldsymbol{z} = 0$, where $\boldsymbol{z} = [q,\ \psi,\ \vartheta]^T$.

For such a form, where $\mathbf{A}$ and $\mathbf{B}$ are constant matrices, one obtains [15] using the Shapiro-Loginov theorem [34]

$$(\mathbf{1}d/dt + \mathbf{C}) \begin{pmatrix} \langle \boldsymbol{z} \rangle \\ \langle E_t^{DMP} \boldsymbol{z} \rangle \end{pmatrix} = 0, \mathbf{C} = \begin{pmatrix} \mathbf{A} & \mathbf{B} \\ E^2 \mathbf{B} & \mathbf{A} + 2\alpha \mathbf{1} \end{pmatrix}. \tag{4}$$

In our case, $\mathbf{A}$ and $\mathbf{B}$ are 3×3 matrices, where $A_{11} = 1/T_q$, $A_{12} = \sigma_H E_1$, $A_{13} = q_\vartheta/T_q$, $A_{21} = a E_1$, $A_{22} = \Lambda_1 - \Lambda_2 (E_1^2 + E^2)$, $A_{23} = b E_1$, $A_{31} = e_q/\gamma_1$, $A_{32} = e_\psi/\gamma_1$, $A_{33} = 1/T_\vartheta$, $B_{11} = B_{13} = B_{31} = B_{33} = 0$, $B_{12} = \sigma_H$, $B_{21} = a$, $B_{22} = -2\Lambda_2 E_1$, $B_{23} = b$, $B_{32} = e_\psi/\gamma_1$. For Λ_1 and Λ_2 see Appendix A. $\langle \cdots \rangle$ denotes the average of the enclosed expression over all possible realizations of the stochastic process.

2.1. Constant field

Recent experiments have confirmed that nematic liquid crystals under DC excitation show a rich spectrum of patterns similar to those obtained for deterministic sinusoidal or stochastic excitation. Grid patterns (called hexagonal patterns) have been observed above a first threshold for the DC field [35, 36]. Beyond a second threshold the hexagonal convective structure starts to oscillate in coherent domains [35, 36]. Other types of domain oscillations, which are self-organized in space as concentric or spiral phase waves, were also found [27, 28]. The transition to turbulence has also been investigated experimentally [28].

These experiments have provided the motivation for consideration of the case of a constant driving field, $E_t = E_1 = \text{const}$. We determine the thresholds for the appearance of both normal and oblique rolls for a wide range of the anisotropic conductivity $\sigma_\parallel/\sigma_\perp$ and for different strengths of the flexoeffect.

The eigenvalues λ of the system (1–3) are determined by a cubic equation, $\sum_{n=0}^{3} a_n \lambda^n = 0$. The Hurwitz criterion yields that $a_0 = 0$ gives the neutral curve $E_1^2(\delta)$ for a stationary bifurcation. Below this curve $\mathrm{Re}\{\lambda\} < 0$ holds for all eigenvalues λ, whereas above at least one eigenvalue exists with a real part greater than zero. Minimizing E_1^2 with respect to δ gives the threshold

$$E_1^2 = \inf_{\delta} \frac{\Lambda_1(e_q q_\vartheta T_\vartheta - \gamma_1)}{a(e_\psi q_\vartheta T_\vartheta - \gamma_1 T_q \sigma_H) - b T_\vartheta (e_\psi - e_q T_q \sigma_H) + \Lambda_2 (e_q q_\vartheta T_\vartheta - \gamma_1)}, \tag{5}$$

see Fig. 2. All thresholds increase with decreasing value of $\sigma_\parallel/\sigma_\perp$. The threshold for normal rolls ($\delta = 0$) is not affected by the flexoeffect since all flexoelectric terms couple to $\sin\delta$ (confer Appendix A) and, therefore, vanish for $\delta = 0$. For $\lambda_- = \lambda_+ = \lambda_{+/-} = 0$ (no flexoeffect) oblique rolls have a lower threshold than normal rolls below a critical anisotropic conductivity $\sigma_\parallel/\sigma_\perp \simeq 1.14$. Above this value the threshold for normal rolls shows the known *divergent* behaviour for $\sigma_\parallel/\sigma_\perp \to 1$ [37]. Following the meaning in [19] we call such a critical point for the oblique-normal rolls transition Lifshitz point. The corresponding $+\delta$-branch of the pitchfork bifurcation for $\lambda_{+/-} = 0$ is shown by the lower picture in Fig. 2.

When the flexoeffect is included the appearence of the patterns changes significantly. Oblique rolls have now a lower threshold than normal rolls for all $\sigma_\parallel/\sigma_\perp \geq 1$ (see graphs (*a*)–(*e*) in Fig. 2) . Therefore there is no oblique-normal rolls transition for decreasing anisotropy in the conductivity; oblique rolls are favoured by the flexoeffect. A remarkable consequence of the flexoeffect is a *finite* threshold for oblique rolls even for *isotropic* conductivity $\sigma_\parallel/\sigma_\perp = 1$. These features are not affected qualitatively, and only slightly quantitatively, by an error-based variation for the values of $(e_1 + e_3)$ and $(e_1 - e_3)$ (see graphs (*b*)-(*e*) in Fig. 2) .

Using the standard values for the material parameters of MBBA [19] and $\lambda_+ = \lambda_- = \lambda_{+/-} = 1$ the angle δ decreases from $\delta = 52.4^\circ$ at $\sigma_\parallel/\sigma_\perp = 2$ to its minimum of

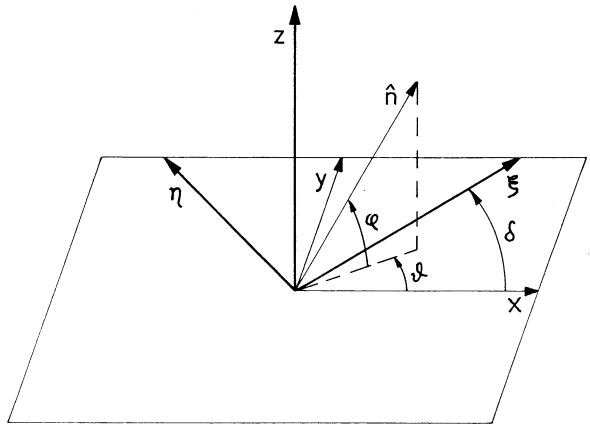

Fig. 1. Illustration of the coordinate systems and angles used

$\delta = 50.8^\circ$ at $\sigma_\parallel/\sigma_\perp = 1.4$. For smaller values of $\sigma_\parallel/\sigma_\perp$ the angle δ increases monotonically and ends with $\delta = 56.6^\circ$ at $\sigma_\parallel/\sigma_\perp = 1$ (graph (*a*) in Fig. 2) . For $\sigma_\parallel/\sigma_\perp = 1.5$ the critical voltage is $U_1 \simeq 1.72\,\mathrm{V}$ and $\delta = 51.0^\circ$ in agreement with [21].

In three-dimensional calculations with "fully rigid" boundary conditions a divergent behaviour of the threshold for $\sigma_\parallel/\sigma_\perp \to 1$ is reported [21], but a finite threshold at $\sigma_\parallel/\sigma_\perp = 1$ is mentioned, too [19]. We find a finite result in our quasi one-dimensional model and now investigate the underlying mechanism in more detail.

For $\sigma_\parallel/\sigma_\perp = 1$ the instability is triggered by the *flexoelectric* charge density

$$q_{FL} = \mathrm{div}\, \boldsymbol{P}_{FL} = -\lambda_+ \sin\delta \cos\delta (e_1 + e_3)\, k_\xi^2 \vartheta\,, \tag{6}$$

which plays a role similar to the space charge density in the Carr-Helfrich mechanism for $\sigma_\parallel/\sigma_\perp = 1$. The η- and z-components of the torque balance equation for isotropic conductivity and isotropy in the dielectric constants $(\varepsilon_\parallel/\varepsilon_\perp = 1)$ are

$$\tfrac{1}{2}\cos\delta(\gamma_1 - \gamma_2)\,\partial_\xi v_z + \lambda_-(e_1 - e_3)\sin\delta\;\partial_\xi \vartheta \mathrm{E}_1 = -(K_{33}\cos^2\delta + K_{22}\sin^2\delta)\,\partial_{\xi\xi}\varphi, \tag{7}$$

$$\lambda_-(e_1 - e_3)\sin\delta\;\partial_\xi\varphi\, E_1 = (K_{33}\cos^2\delta + K_{11}\sin^2\delta)\,\partial_{\xi\xi}\vartheta. \tag{8}$$

At the threshold the destabilizing viscous and flexoelectric torque (left-hand side) equals the stabilizing elastic torque (right-hand side). The lowering of the threshold is plausible since the destabilizing flexoelectric torque increases with $\sin\delta$ (provided $(e_1 - e_3) \neq 0$) and dominates the stabilizing elastic torque, which increases with $\sin^2\delta$.

Exploiting the z-component of the Navier-Stokes equation we eliminate $\partial_\xi v_z$ and obtain

$$E_1^2\Big|_{\frac{\sigma_\parallel}{\sigma_\perp}=\frac{\varepsilon_\parallel}{\varepsilon_\perp}=1} = \inf_\delta \frac{k_\xi^2(K_{33}\cos^2\delta + K_{11}\sin^2\delta)(K_{33}\cos^2\delta + K_{22}\sin^2\delta)}{\sin^2\delta[\lambda_-(e_1-e_3)-(\gamma_1-\gamma_2)\cos^2\delta\lambda_+(e_1+e_3)/(2\eta_1)]\lambda_-(e_1-e_3)}\,, \tag{9}$$

which reproduces the previous result (5) for $\sigma_\parallel/\sigma_\perp = \varepsilon_\parallel/\varepsilon_\perp = 1$. Beyond this threshold the destabilizing torque dominates, small director fluctuations are amplified, and the oblique rolls appear.

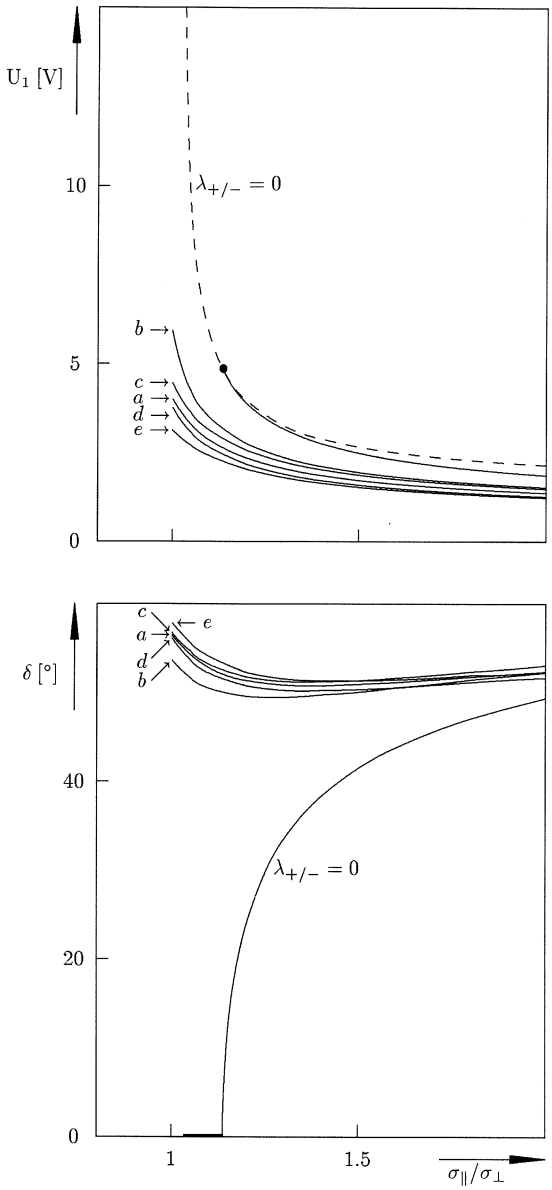

Fig. 2. Excitation with constant field. DC thresholds and oblique rolls angle δ against the anisotropy of the conductivity $\sigma_\parallel/\sigma_\perp$ for normal rolls (dashed line) and oblique rolls (solid line) at various strengths of the flexoeffect. Without flexoelectric effect ($\lambda_{+/-}=0$) the Lifshitz point (●) of the oblique-normal transition occurs at $\sigma_\parallel/\sigma_\perp \simeq 1.14$. The behaviour of the threshold for the standard strength of the flexoeffect ($\lambda_{+/-}=1$) is shown in graph *a*. An error-based variation of the strength does not cause any qualitative changes as the graphs *b* ($\lambda_+ = 0.7$, $\lambda_- = 0.9$), *c* ($\lambda_+ = 0.7$, $\lambda_- = 1.1$), *d* ($\lambda_+ = 1.3$, $\lambda_- = 0.9$), and *e* ($\lambda_+ = 1.3$, $\lambda_- = 1.1$) show. Material parameters were taken from [21]

2.2. Pure stochastic excitation

For pure stochastic excitation, $E_t = E_t^{DMP}$, the characteristic equation which determines the eigenvalues λ of $-\mathbf{C}$ given by (4) is a product of two cubic equations $P^{(1)}(\lambda)\cdot P^{(2)}(\lambda)=0$. As before $a_0^{(1,2)}=0$ give two neutral curves,

$$E_{n,1}^2(\delta) = \frac{\Lambda_1}{N}\,[T_\vartheta(4\alpha^2\gamma_1 T_q + 2\alpha\gamma_1 - e_q q_\vartheta) + \gamma_1(2\alpha T_q + 1)], \tag{10}$$

where $N = e_\psi T_\vartheta[b(2\alpha T_q+1) - aq_\vartheta] + T_\vartheta[\Lambda_2(4\alpha^2\gamma_1 T_q + 2\alpha\gamma_1 - e_q q_\vartheta) + T_q\sigma_H(2a\alpha\gamma_1 - be_q)] + \gamma_1[\Lambda_2(2\alpha T_q+1) + aT_q\sigma_H]$, and

$$E_{n,2}^2(\delta) = \frac{(e_q q_\vartheta T_\vartheta - \gamma_1)(2\alpha+\Lambda_1)}{a(e_\psi q_\vartheta T_\vartheta - \gamma_1 T_q\sigma_H) - bT_\vartheta(e_\psi - e_q T_q\sigma_H) + \Lambda_2(e_q q_\vartheta T_\vartheta - \gamma_1)}. \tag{11}$$

The threshold $E^2 = \min[\inf_\delta E_{n,1}^2(\delta), \inf_\delta E_{n,2}^2(\delta)]$ and the corresponding angle δ of the oblique rolls are shown in Fig. 3 as functions of the mean frequency α for $\lambda_{+/-}=0$ and 1. The critical frequency α_c separating "conductive" and "dielectric" regimes is defined by $\inf_\delta E_{n,1}^2(\delta) = \inf_\delta E_{n,2}^2(\delta)$.

The gross behaviour of the threshold is similar to that obtained for deterministic square wave excitation [17, Fig. 1] and for deterministic sinusoidal excitation [19, Fig. 3; 20, Fig. 1]. Practically independent from the strength of flexoeffect we find for $\alpha < \alpha_L$ oblique rolls and for $\alpha_L < \alpha < \alpha_C$ normal rolls (α_L is the Lifshitz frequency indicating the oblique-normal rolls transition). For $\alpha > \alpha_c$ and $\lambda_{+/-}=1$ we find again oblique rolls. (In the range from $\alpha = 5\cdot 10^2\,\mathrm{s}^{-1} \cdots 10^4\,\mathrm{s}^{-1}$ the angle δ of the oblique rolls decreases by only $8.7\cdot 10^{-3}$ deg.)

In the experiment, hitherto, oblique rolls have been observed only for deterministic (sinusoidal) excitation in the conductive regime [9]. We therefore propose a careful inspection of the first pattern against which the homogeneous state becomes unstable for pure stochastic excitation.

2.3. Superposition

For the superposition of a constant and a stochastic field, $E_t = E_1 + E_t^{DMP}$, the eigenvalues of $-\mathbf{C}$ given by (4) are

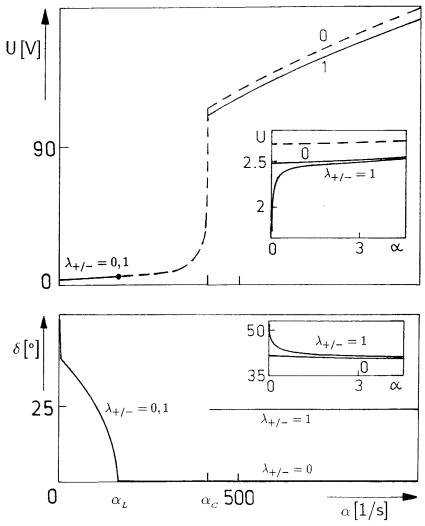

Fig. 3. Pure stochastic excitation. Thresholds for normal rolls and oblique rolls (dashed and solid lines, respectively) and characteristic angle δ of the oblique rolls for different strengths of the flexoeffect against mean frequency α. Without flexoeffect, oblique rolls appear only for small α. In this region (with the exception of very small α, see also insertion) the threshold curves and Lifshitz points (●) practically coincide for $\lambda_{+/-} = 0$ and 1. Material parameters were taken from [21] and $\sigma_\parallel = 1.5 \cdot 10^{-10} \Omega^{-1} \mathrm{cm}^{-1}$

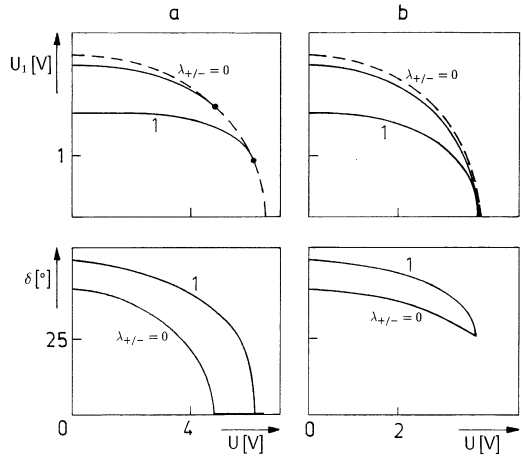

Fig. 4a, b. Superposition of constant and stochastic field at $\alpha = 10^2 \, \mathrm{s}^{-1}$ where the noise is always destabilizing. Thresholds for normal rolls and oblique rolls are shown as the dashed and solid lines, respectively and oblique rolls angle δ for different strengths of the flexoeffect against stochastic voltage. ● denotes the Lifshitz points. Material parameters were taken from [21] with $\sigma_\parallel = 6.0 \cdot 10^{-11} \Omega^{-1} \mathrm{cm}^{-1}$ **a** and $\sigma_\parallel = 1.5 \cdot 10^{-10} \Omega^{-1} \mathrm{cm}^{-1}$ **b**

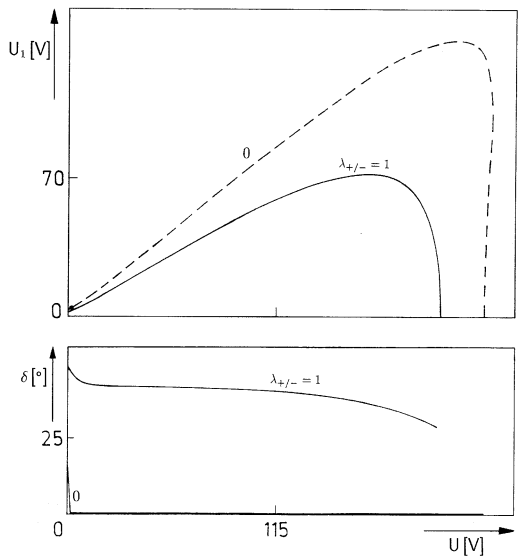

Fig. 5. Superposition of constant and stochastic field at $\alpha = 10^3 \mathrm{s}^{-1}$. Thresholds for normal rolls and oblique rolls are shown as the dashed and solid lines, respectively and oblique rolls angle δ for different strengths of the flexoeffect against stochastic voltage. ● denotes the Lifshitz points. Material parameters were taken from [22] with $\sigma_\parallel = 6.0 \cdot 10^{-11} \Omega^{-1} \mathrm{cm}^{-1}$

determined by a sixth order equation. The Hurwitz criterion shows that $a_0 = 0$ determines the neutral curve $E_1^2(E^2, \delta)$.

The behaviour of the threshold $E_1^2 = \inf_\delta E_1^2(E^2, \delta)$ depends on the order of the correlation time of the noise, $\tau_{\mathrm{stoch}} = 1/2\alpha$, compared with the relaxation time of the space charge T_q.

For $\tau_{\mathrm{stoch}} \approx T_q$ the stochastic field always destabilizes the homogeneous state. For $\tau_{\mathrm{stoch}} \ll T_q$ the stochastic field stabilizes the homogeneous state as long as its magnitude is not too large. The effect of such a ("fast") stochastic field changes from stabilizing to destabilizing if the field is strong enough. The behaviour of the threshold for E_1 can be smooth or discontinuous. Above a critical strength of the stochastic field the threshold condition may have two solutions for the deterministic field. In this case the threshold curve appears discontinuous if first the stochastic field is applied and then the deterministic field is increased until the structure is established. This general behaviour found in previous work testing the stability only against normal rolls [14–16] remains true if we allow the formation of oblique rolls. Some new aspects are now discussed in detail, see Figs. 4 and 5.

For $\tau_{\mathrm{stoch}} \approx T_q$ we consider two parameter settings with different magnitudes of $\sigma_\parallel$ but $\sigma_\parallel / \sigma_\perp = \mathrm{const}$. For small $\sigma_\parallel$ and for stochastic voltages below a Lifshitz point (Fig. 4a) oblique rolls have the lower threshold, whereas for larger $\sigma_\parallel$ the oblique rolls always have the lowest threshold (Fig. 4b). When reaching the Lifshitz point the angle δ of the oblique rolls tends to zero as expected. Oblique rolls are again favoured by the flexoeffect.

For $\tau_{\mathrm{stoch}} \ll T_q$ and $\lambda_{+/-} = 0$ oblique rolls have only a lower threshold for stochastic voltages below the Lifshitz point . The difference between the thresholds for normal and oblique rolls is, however, very small, $\Delta U_1 \simeq 0.005$ V. For strong flexoeffect, $\lambda_{+/-} = 1$, oblique rolls always give the lowest threshold. In Fig. 5 we have chosen a parameter setting which leads to a discontinuous behaviour of the normal rolls threshold in the absence of the flexoeffect. A detailed investigation of the $\sigma_\parallel / \sigma_\perp$–$\varepsilon_\parallel / \varepsilon_\perp$-plane shows that the discontinuous behaviour can be considered as typical [38]. Changing sligthly only the anisotropy of the dielectric constants from $\varepsilon_\parallel / \varepsilon_\perp = 0.9$ to $\simeq 0.874$ in the material parameters of [22], the threshold

for oblique rolls exhibits a discontinuous behaviour for the standard values of $(e_1 + e_3)$ and $(e_1 - e_3)$, too.

3. Three-dimensional theory

We consider a three-dimensional linear theory which allows the stability of the homogeneous nematic state to be tested against normal rolls as well as oblique rolls, and to determine *two* wave numbers by mode selection. Thus the influence of fixing a wave number, as in the one-dimensional model, can be estimated. The thresholds were calculated for all three types of excitation to realize a complete comparision with the results of the one-dimensional model without the flexoeffect. Oblique rolls are characterized by two wave numbers, k_x and k_y, whereas the normal rolls are described by only one wave number k_x ($k_y \equiv 0$). The disturbed director $\hat{n}$ includes the angle φ with the xy-plane and the angle ϑ with the xz-plane (see Fig. 1). In the coordinate system xyz the variables are the charge density q, and the angles φ and ϑ.

We start with the same set of electrohydrodynamic equations for a nematic liquid crystal as in the one-dimensional description (confer Chap. 2, second paragraph). To simplify the calculations we use unrealistic "fully free" (torque- and stress-free) boundary conditions [12]

$$\partial_z \vartheta = \partial_z v_x = \partial_z v_y = 0 \quad \text{for} \quad z = \pm d/2\,, \tag{12}$$

where v_i $(i = x,\ y,\ z)$ is the i-component of the hydrodynamic velocity for the moving fluid. From experience with deterministic excitation (confer [12], Fig. 3) one expects only a small quantitative change for realistic boundary conditions. From the geometric constraints we see that

$$v_z = \varphi = 0 \quad \text{for} \quad z = \pm d/2. \tag{13}$$

We further exploit incompressibility

$$\operatorname{div} v = 0, \tag{14}$$

and assume

$$\operatorname{rot} \boldsymbol{E} = 0\,. \tag{15}$$

We insert into the full set of hydrodynamic equations a test mode describing an oblique roll with wave numbers (k_x, k_y) which satisfies (12–15). The ansatz for the variables q, φ, and ϑ, the induced electric field $\boldsymbol{E}$, the hydrodynamic velocity $\boldsymbol{v}$, and the pressure p reads

$$q(x, y, z, t) = \tilde{q}(t) \sin(k_x x + k_y y) \cos k_z z, \tag{16}$$

$$\varphi(x, y, z, t) = \tilde{\varphi}(t) \cos(k_x x + k_y y) \cos k_z z, \tag{17}$$

$$\vartheta(x, y, z, t) = \tilde{\vartheta}(t) \sin(k_x x + k_y y) \sin k_z z, \tag{18}$$

$$E_x(x, y, z, t) = \tilde{E}_{\text{ind}}(t) \cos(k_x x + k_y y) \cos k_z z\,, \tag{19}$$

$$E_y(x, y, z, t) = \frac{k_y}{k_x} \tilde{E}_{\text{ind}}(t) \cos(k_x x + k_y y) \cos k_z z, \tag{20}$$

$$E_z(x, y, z, t) = -\frac{k_z}{k_x} \tilde{E}_{\text{ind}}(t) \sin(k_x x + k_y y) \sin k_z z, \tag{21}$$

$$v_x(x, y, z, t) = \frac{1}{k_x}[\tilde{v}_y(t) k_y - \tilde{v}_z(t) k_z \cos(k_x x + k_y y) \sin k_z z, \tag{22}$$

$$v_y(x, y, z, t) = -\tilde{v}_y(t) \cos(k_x x + k_y y) \sin k_z z, \tag{23}$$

$$v_z(x, y, z, t) = \tilde{v}_z(t) \sin(k_x x + k_y y) \cos k_z z, \tag{24}$$

$$p(x, y, z, t) = \tilde{p}(t) \sin(k_x x + k_y y) \sin k_z z. \tag{25}$$

v_x and E_z are choosen such that the conditions (14) and (15) are fulfilled. An oblique roll with $(k_x,\ -k_y)$ gives the same threshold. A superposition of rolls with (k_x, k_y) and $(k_x,\ -k_y)$ can be considered as an ansatz for a rhombic cell (see Appendix B). As before we use oblique rolls as a synonym for both patterns. The chosen ansatz is more general in the z-dependence of the quantities than those in [12, 21]. This general form prevents the inclusion of the flexoeffect in our three-dimensional calculations in a way which ends with coupled ordinary differential equations as in the case of the one-dimensional model (see equations (1–3)). Therefore we compare only the three-dimensional results and the one-dimensional results *without* the flexoeffect.

From the continuity equation, $\dot{q} + \operatorname{div} \boldsymbol{j} = 0$, one obtains with (16, 17, 19–21) a linearized differential equation for $\tilde{q}$ where $\tilde{E}_{\text{ind}}(t)$ is eliminated with the help of Maxwell's equation $\operatorname{div} \boldsymbol{D} = 4\pi q$. Inserting equations (17, 18, 22-25) the x-, y-, and z-components of the Navier-Stokes equation represent a linear inhomogeneous system for $\tilde{p}(t)$, $\tilde{v}_y(t)$, and $\tilde{v}_z(t)$. The resulting terms for $\tilde{v}_y(t)$, $\tilde{v}_z(t)$, and $\tilde{E}_{\text{ind}}(t)$ (from Maxwell's equation), substituted in the y- and z-component of the torque balance equation, yield a linear inhomogeneous system of equations for $\dot{\tilde{\varphi}}$ and $\dot{\tilde{\vartheta}}$.

The linearized electrohydrodynamic equations in 3 dimensions describing the stability against 3-dimensional structures formed by normal or oblique rolls read (from now tildes are omitted)

$$\dot{q} + \frac{1}{T_q} q + \sigma_H k_x E_t \varphi = 0, \tag{26}$$

$$\dot{\varphi} + a E_t q + \frac{1}{T_\varphi} \varphi + b \vartheta = 0, \tag{27}$$

$$\dot{\vartheta} + c E_t q + d\varphi + \frac{1}{T_\vartheta} \vartheta = 0. \tag{28}$$

$1/T_\varphi$ depends on the square of the driving field E_t as well as on the wave numbers k_x, k_y, and k_z, as given in Appendix C. The other coefficients (see Appendix C) contain material constants and depend on the characteristic parameters k_x, k_y, and k_z of the test mode. The boundary conditions (12, 13) are fulfilled by $k_z = (2n + 1)\,\pi/d$, $n = 0$, 1, … . Since $n = 0$ leads to the lowest threshold we choose $k_z = \pi/d$. The wave numbers k_x and k_y are determined numerically. The oblique rolls include the angle $\delta = \arctan(k_y/k_x)$ with the y-axis.

For the derivation of (26–28) we have neglected the diffusion currents. This is allowed as long as $(k/T_q D)^2 \ll 1$ holds [29] which we checked numerically for all parameter sets used (D is the diffusion constant of the liquid crystal and k the wave number perpendicular to the respective roll pattern).

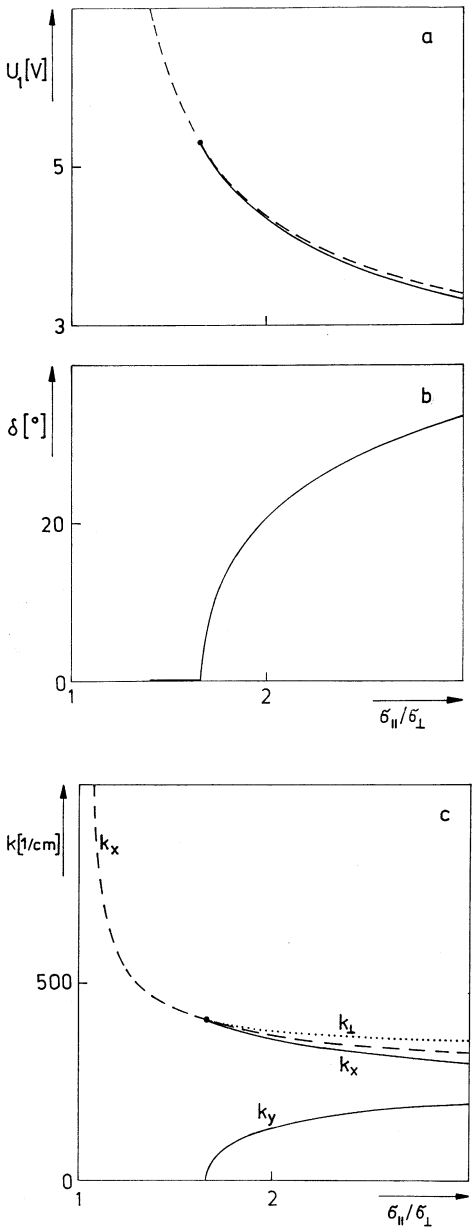

Fig. 6a–c. Excitation with constant field for different $\sigma_\parallel/\sigma_\perp$. **a** shows the thresholds for normal rolls (dashed line) and oblique rolls (solid line). The characteristic angle δ of the oblique rolls structure is plotted in **b**. In **c** the selected wave numbers k_x, k_y for oblique rolls (solid line), k_x for normal rolls (dashed line), and the wave number perpendicular to the oblique rolls $k_\perp$ (dotted line) are shown. ● denotes the Lifshitz point. Material parameters were taken from [22]

To investigate the stability of the first moments according to (4) we write (26–28) in matrix form, $\dot{z} + (\mathbf{A} + \mathbf{B}E_t^{DMP})\, z = 0$, with $z = [q, \varphi, \vartheta]^T$. Here, $\mathbf{A}$ and $\mathbf{B}$ are constant 3×3 matrices, where $A_{11} = 1/T_q$, $A_{12} = \sigma_H k_x E_1$, $A_{13} = 0$, $A_{21} = aE_1$, $A_{22} = \Lambda_1 - \Lambda_2 (E_1^2 + E^2)$, $A_{23} = b$, $A_{31} = cE_1$, $A_{32} = \Lambda_3 + \Lambda_4(E_1^2 + E^2)$, $A_{33} = 1/T_\vartheta$, $B_{11} = 0$, $B_{12} = \sigma_H k_x$, $B_{13} = 0$, $B_{21} = a$, $B_{22} = -2\Lambda_2 E_1$, $B_{23} = 0$, $B_{31} = c$, $B_{32} = 2\Lambda_4 E_1$, $B_{33} = 0$. For Λ_1, Λ_2, Λ_3, and Λ_4 see Appendix C.

3.1. Constant field

We first consider the case of a constant driving field, $E_t = E_1 = \text{const.}$, and determine the threshold for the appearance of both normal and oblique rolls for different strengths of the anisotropy of conductivity $\sigma_\parallel/\sigma_\perp$.

The eigenvalues λ of the system (26–28) are determined by a cubic equation, $\sum_{n=0}^{3} a_n \lambda^n = 0$. The Hurwitz criterion shows that the neutral surface over the k_x-k_y-plane $E_1^2(k_x, k_y)$ is given by $a_0 = 0$, the condition for a stationary bifurcation. The global minimum of the surface gives the threshold

$$E_1^2 = \inf_{k_x, k_y} \frac{\Lambda_1 - \Lambda_3 T_\vartheta b}{a k_x \sigma_H T_q - b T_\vartheta [c k_x T_q \sigma_H - \Lambda_4] + \Lambda_2}, \tag{29}$$

see Fig. 6.

The thresholds for normal and oblique rolls increase with decreasing anisotropy of conductivity. For stronger anisotropy oblique rolls are favoured and the corresponding angle δ increases monotonically for $\sigma_\parallel/\sigma_\perp$ beyond the Lifshitz point. For the same parameters, the distance between oblique rolls is smaller than between normal rolls, as a comparison of k_x with $k_\perp$ (wave number perpendicular to the oblique rolls) shows. This is observed for all three kinds of excitation. At the Lifshitz point ($\delta \to +0$) $k_\perp$ becomes equal to k_x (see Fig. 6c), i.e. there is a change from the homogeneous state-oblique rolls transition to the homogeneous state-normal rolls transition.

3.2. Pure stochastic excitation

For pure stochastic excitation, $E_t = E_t^{DMP}$, the characteristic equation determining the eigenvalues of $-\mathbf{C}$ separates into a product of two cubic equations $P^{(1)}(\lambda) \cdot P^{(2)}(\lambda) = 0$. As before $a_0^{(1,2)} = 0$ gives two neutral surfaces,

$$E_{n,1}^2(k_x, k_y) = \frac{(\Lambda_1 - \Lambda_3 b T_\vartheta)\ (2\alpha T_q + 1)}{2\alpha T_q (\Lambda_2 - \Lambda_4 b T_\vartheta) + a k_x T_q \sigma_H - k_x b c T_q T_\vartheta \sigma_H + \Lambda_2 - \Lambda_4 b T_\vartheta}, \tag{30}$$

$$E_{n,2}^2(k_x, k_y) = \frac{4\alpha^2 T_\vartheta + 2\alpha(\Lambda_1 T_\vartheta + 1) + \Lambda_1 - \Lambda_3 b T_\vartheta}{2\alpha T_\vartheta (a k_x T_q \sigma_H + \Lambda_2) + a k_x T_q \sigma_H - k_x b c T_q T_\vartheta \sigma_H + \Lambda_2 + \Lambda_4 b T_\vartheta}. \tag{31}$$

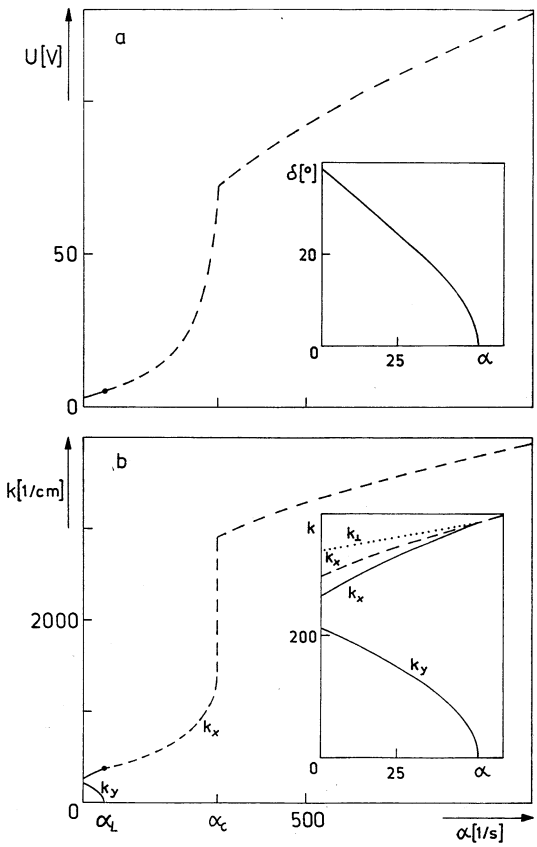

Fig. 7a, b. Pure stochastic excitation with dichotomous noise of different mean frequencies α. In **a** thresholds for normal rolls and oblique rolls (dashed and solid line, respectively) and the oblique rolls angle δ (insertion) are shown. Oblique rolls appear only for small α; the oblique rolls angle δ decreases monotonically with increasing α. In **b** the wave numbers k_x, k_y (solid lines), and $k_\perp$ (dotted line) for oblique rolls and k_x for normal rolls (dashed line) are given. The insertion shows the behaviour for small α. The wave number for normal rolls k_x increases drastically at the transition frequency from "conductive" to "dielectric" regime. • denotes the Lifshitz point. Material parameters were taken from [21] with exception of $\sigma_\parallel/\sigma_\perp = 3.0$ where $\sigma_\parallel = 6.0 \cdot 10^{-11} \Omega^{-1}\text{cm}^{-1}$

The threshold $E^2 = \min[\inf_{k_x,k_y} E^2_{n,1}(k_x, k_y), \inf_{k_x,k_y} E^2_{n,2}(k_x, k_y)]$, the selected angle δ, and the wave numbers k_x, k_y, and $k_\perp$ are shown in Fig. 7 as functions of the mean frequency α. The critical frequency α_c separating "conductive" and "dielectric" regimes is defined by $\inf_{k_x,k_y} E^2_{n,1}(k_x, k_y) = \inf_{k_x,k_y} E^2_{n,2}(k_x, k_y)$.

For small α the behaviour of the threshold is similar (slowly increasing linearly) to that for deterministic sinusoidal excitation (confer [12], Fig. 3). Oblique rolls are favoured for noise frequencies smaller than the Lifshitz frequency. The difference to the threshold for normal rolls is smaller than in the one-dimensional model caused by k_x-wave numbers which are larger than π/d. For instance for $\alpha = 0.7\,\text{s}^{-1}$ the difference drops from $\Delta U_{\text{one-dim.}} = 382\,\text{mV}$ to $\Delta U_{\text{three-dim.}} = 108\,\text{mV}$. Higher k_x-wave numbers also yield higher thresholds in the "dielectric" regime with a difference of about 4V to the one-dimensional threshold. At α_c the wave number for normal rolls k_x increases drastically as in the two-dimensionl theory for pure stochastic excitation [16, Fig. 4] and there is a similiar behaviour for deterministic sinusoidal excitation [19, Fig. 3].

3.3. Superposition

For the superposition of a constant and a stochastic field, $E_t = E_1 + E_t^{DMP}$, the eigenvalues of $-\mathbf{C}$ are determined by a sixth order equation. The Hurwitz criterion shows again that $a_0 = 0$ gives the neutral surface $E_1^2(E^2, k_x, k_y)$. The threshold $E_1^2 = \inf_{k_x,k_y} E_1^2(E^2, k_x, k_y)$ behaves in a characteristic way depending on the order of the correlation time of the noise τ_{stoch} compared with the characteristic time T_q.

For $\tau_{\text{stoch}} \approx T_q$ oblique rolls always have the lowest threshold below the Lifshitz point (Fig. 8a) which exists for all parameter settings used. For increasing strength of the stochastic voltage the oblique rolls angle δ decreases monotonically and becomes zero at the Lifshitz point (Fig. 8b).

For $\tau_{\text{stoch}} \ll T_q$ we have chosen a parameter setting which leads to a discontinuous behaviour of the threshold for normal rolls. Oblique rolls have a lower threshold for stochastic voltages below the Lifshitz point (Fig. 9a). The difference between the thresholds for normal and oblique rolls is very small, $\Delta U \leq 0.06\,\text{V}$. In contrast to the one-dimensional model (see Fig. 5) the selected angle δ reaches a maximum for increasing strength of stochastic field, and then tends to zero (Fig. 9b).

4. Concluding remarks

We found that in the frame of a quasi one-dimensional theory, for a certain parameter range of the stochastic field, oblique rolls have a lower threshold than normal rolls. The flexoeffect favours the formation of oblique rolls. There are, however, no experimental reports about oblique rolls for stochastically driven nematics [1–7].

The 3-dimensional theory predicts the appearance of oblique rolls for a certain parameter range of the driving field, as well. In addition it is found that the roll cell pattern becomes narrower both with increasing strength of the stochastic field and with increasing mean frequency α, as found for normal rolls in a two-dimensional theory [16].

For stochastically driven systems there exist different stability criteria: the bifurcation of the most probable value [39], the stability of the first and higher moments [40] or the sample stability [41]. It is not clear a priori which criterion best applies to the experimental measurements. We have addressed this problem in other publications [16, 42] and it turns out that the different stability criteria give similar results if the characteristic times of the system and the noise are well separated. According to this result we chose the stability criterion of the first moments since it is much less laborious and reflects sufficiently the behaviour of the threshold for the homogeneous nematic state.

To achieve a description of other experimentally observed noise induced phenomena, such as the alteration of the bifurcation sequence and a noise induced hysteresis it

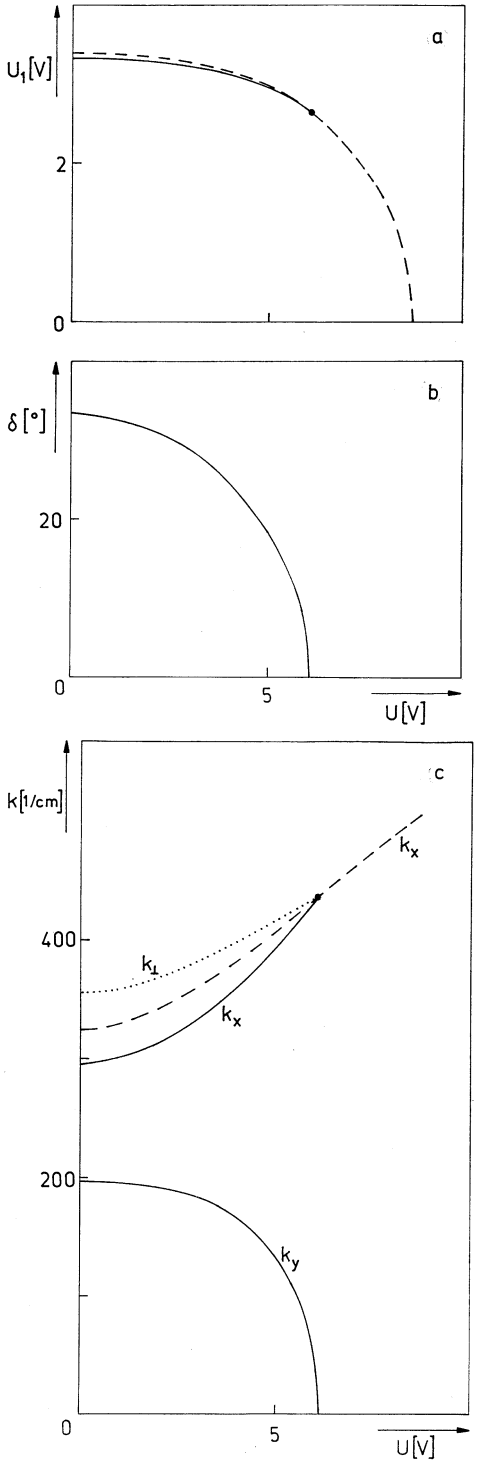

Fig. 8a–c. Superposition of constant and stochastic field at $\alpha = 10^2 s^{-1}$ where the noise is always destabilizing. Thresholds and oblique rolls angle are shown in **a** and **b**. Wave numbers k_x, k_y (solid lines), and $k_\perp$ (dotted line) for oblique rolls and k_x for normal rolls (dashed line) are plotted in **c**. For small stochastic fields the oblique rolls (solid line) are favoured which merge at the Lifshitz point (●) into the normal rolls (dashed line). Material parameters were taken from [22] with exception of $\sigma_\parallel/\sigma_\perp = 3.0$ where $\sigma_\parallel = 6.0 \cdot 10^{-11}$ $\Omega^{-1}\text{cm}^{-1}$

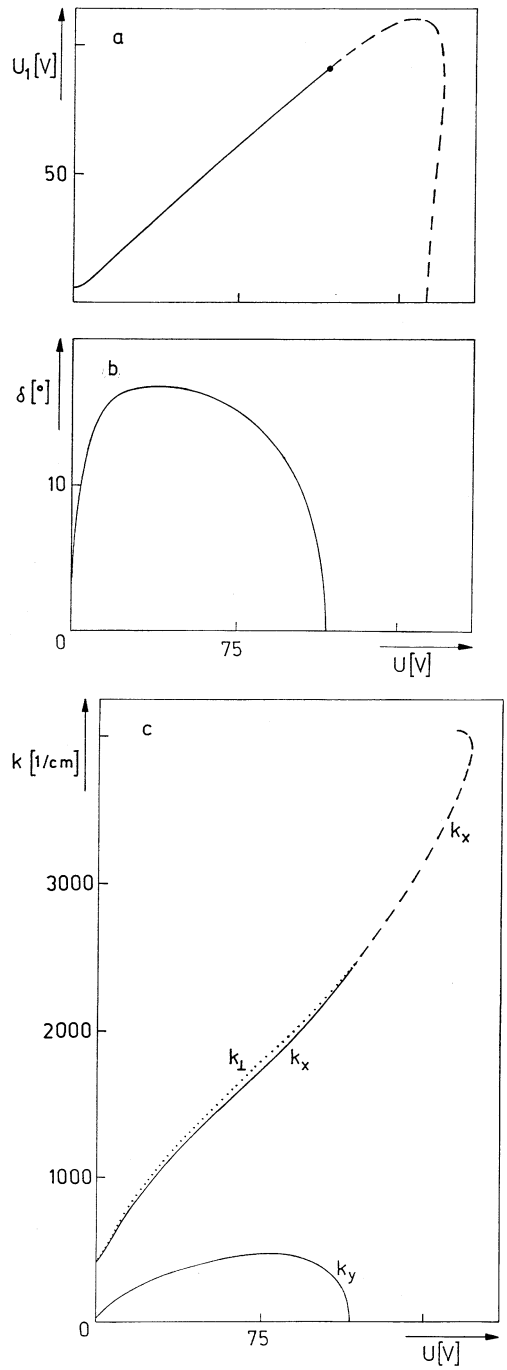

Fig. 9a–c. Superposition of constant and stochastic field at $\alpha = 10^3 s^{-1}$. Thresholds for normal rolls and oblique rolls (dashed and solid lines, respectively) are shown in **a**. The oblique roll's angle δ is plotted in **b**. **c** shows the wave numbers k_x, k_y (solid lines), and $k_\perp$ (dotted line) for oblique rolls and k_x for normal rolls above the Lifshitz point (dashed line). ● denotes the Lifshitz point. Material parameters were taken from [21] with exception of $\sigma_\parallel/\sigma_\perp = 1.8$ where $\sigma_\parallel = 1.5 \cdot 10^{-10} \Omega^{-1}\text{cm}^{-1}$, $\varepsilon_\parallel = 3.95$, and $\varepsilon_\perp = 5.25$

is essential to consider a nonlinear theory. We conjecture that the alteration of the bifurcation sequence (which means that the threshold towards, e.g., grid pattern is lower than towards rolls) could be caused by a noise induced change from supercritical to

subcritical bifurcation (confer [6] p. 1149 and [7] p. 64).

In a different context, in the frame of a generalized Swift-Hohenberg model, a noise induced change from supercritical to subcritical bifurcation has been reported [43]. The same phenomenon was found in an extended Stratonovich model, where the noise couples to both the linear and the cubic term [44].

Whereas an analysis of the full nonlinear electrohydrodynamic equations does not seem to be feasible, one could consider a phenomenological description by Ginzburg-Landau equations with *ad hoc* stochastic coefficients. This is appropriate since the *derivation* of amplitude equations from the basic electrohydrodynamic equations with a stochastic electric field is a more subtle problem.

We are grateful to Agnes Buka, Lorenz Kramer, Adolf Kühnel, and Walter Zimmermann for valuable discussions. This work was partially supported by the Deutsche Forschungsgemeinschaft in the frame of the Schwerpunktprogramm "Strukturbildung in dissipativen kontinuierlichen Systemen" under grant Be1417/3.

Appendix A

In the following we give the explicit form of the coefficients of system (1–3). Note the dependence of the *effective* material parameters and characteristic times on both oblique rolls angle δ and wave number k_ξ. For $e_1 = e_3 = \delta = 0$ the one-dimensional theory describing normal rolls [29] is reproduced. Λ_1 and Λ_2 are defined in (A4).

$$\frac{1}{T_q} = \frac{4\pi(\sigma_\perp + \sigma_a \cos^2\delta)}{\varepsilon_\perp + \varepsilon_a \cos^2\delta} \tag{A1}$$

$$\sigma_H = \cos\delta\left[\sigma_a - \frac{\sigma_\perp + \sigma_a\cos^2\delta}{\varepsilon_\perp + \varepsilon_a\cos^2\delta}\varepsilon_a\right] \tag{A2}$$

$$q_\vartheta = \lambda_+ \sin\delta\cos\delta(e_1 + e_3)\, k_\xi^2 \tag{A3}$$

$$\frac{1}{T_\psi} = \Lambda_1 - \Lambda_2 E_t^2 = \frac{k_\xi^2}{\eta}(K_{22}\sin^2\delta + K_{33}\cos^2\delta) - \frac{\varepsilon_a\varepsilon_\perp}{4\pi\eta(\varepsilon_\perp + \varepsilon_a\cos^2\delta)}E_t^2 \tag{A4}$$

$$a = \frac{1}{\eta}\left[\frac{\cos\delta(\gamma_1 - \gamma_2)}{2\eta_1} - \frac{\varepsilon_a\cos\delta}{\varepsilon_\perp + \varepsilon_a\cos^2\delta}\right] \tag{A5}$$

$$b = \left[\lambda_-(e_1 - e_3) - \frac{\varepsilon_a\cos^2\delta}{\varepsilon_\perp + \varepsilon_a\cos^2\delta}\lambda_+(e_1 + e_3)\right]\frac{\sin^2\delta k_\xi^2}{\eta} \tag{A6}$$

$$\frac{1}{T_\vartheta} = \frac{k_\xi^2}{\gamma_1}\left[K_{11}\sin^2\delta + K_{33}\cos^2\delta + \frac{4\pi\lambda_+^2(e_1 + e_3)^2\sin^2\delta\cos^2\delta}{\varepsilon_\perp + \varepsilon_a\cos^2\delta}\right] \tag{A7}$$

$$e_q = \lambda_+\left[\frac{4\pi(e_1 + e_3)\ \sin\delta\cos\delta}{\varepsilon_\perp + \varepsilon_a\cos^2\delta}\right] \tag{A8}$$

$$e_\psi = \left[\lambda_-(e_1 - e_3)\sin\delta - \frac{\lambda_+(e_1 + e_3)\ \sin\delta\cos^2\delta}{\varepsilon_\perp + \varepsilon_a\cos^2\delta}\varepsilon_a\right] \tag{A9}$$

$$\eta = \gamma_1 - \cos^2\delta\,\frac{(\gamma_1 - \gamma_2)^2}{4\eta_1},$$

$$\eta_1 = \tfrac{1}{2}[\alpha_4 - \cos^2\delta\,\gamma_2 + \tfrac{1}{2}\cos^2\delta(\beta + \gamma_1)] \tag{A10}$$

Appendix B

The test mode for rhombic cells resulting from a superposition of two oblique rolls with wave numbers (k_x, k_y) and $(k_x, -k_y)$ is given by

$$q(x, y, z, t) = \tilde{q}(t)\sin k_x x\cos k_y y\cos k_z z, \tag{B1}$$

$$\varphi(x, y, z, t) = \tilde{\varphi}(t)\cos k_x x\cos k_y y\cos k_z z, \tag{B2}$$

$$\vartheta(x, y, z, t) = \tilde{\vartheta}(t)\cos k_x x\sin k_y y\sin k_z z, \tag{B3}$$

$$E_x(x, y, z, t) = \tilde{E}_{\text{ind}}(t)\cos k_x x\cos k_y y\cos k_z z\ , \tag{B4}$$

$$E_y(x, y, z, t) = -\frac{k_y}{k_x}\tilde{E}_{\text{ind}}(t)\sin k_x x\sin k_y y\cos k_z z\ , \tag{B5}$$

$$E_z(x, y, z, t) = -\frac{k_z}{k_x}\tilde{E}_{\text{ind}}(t)\sin k_x x\cos k_y y\sin k_z z\ , \tag{B6}$$

$$v_x(x, y, z, t) = \frac{1}{k_x}\left[\tilde{v}_y(t)\,k_y - \tilde{v}_z(t)\,k_z\right]\cos k_x x\cos k_y y\sin k_z z, \tag{B7}$$

$$v_y(x, y, z, t) = \tilde{v}_y(t)\sin k_x x\sin k_y y\sin k_z z, \tag{B8}$$

$$v_z(x, y, z, t) = \tilde{v}_z(t)\sin k_x x\cos k_y y\cos k_z z, \tag{B9}$$

$$p(x, y, z, t) = \tilde{p}(t)\ \sin k_x x\cos k_y y\sin k_z z\ . \tag{B10}$$

v_x and E_z are chosen such that the conditions (14) and (15) are fulfilled.

Appendix C

The coefficients in the system (26–28) read explicitly

$$\frac{1}{T_q} = 4\pi\frac{\sigma_\parallel k_x^2 + \sigma_\perp(k_y^2 + k_z^2)}{\varepsilon_\parallel k_x^2 + \varepsilon_\perp(k_y^2 + k_z^2)}\ , \tag{C1}$$

$$\sigma_H = \frac{(\sigma_\perp\varepsilon_\parallel - \sigma_\parallel\varepsilon_\perp)\ (k_x^2 + k_y^2 + k_z^2)}{\varepsilon_\parallel k_x^2 + \varepsilon_\perp(k_y^2 + k_z^2)}\ , \tag{C2}$$

$$\mathrm{a} = \frac{m_3 m_6 - m_2 m_7}{m_2 m_5 - m_1 m_6}\ , \tag{C3}$$

$$\frac{1}{T_\varphi} = \Lambda_1 - \Lambda_2 E_t^2 = \frac{(K_{11}k_z^2 + K_{22}k_y^2 + K_{33}k_x^2)\ m_6}{m_2 m_5 - m_1 m_6}$$

$$+\frac{m_2k_yk_z(K_{22}-K_{11})}{m_2m_5-m_1m_6}-\frac{m_6}{m_2m_5-m_1m_6}\times\left[\frac{g_7k_x\varepsilon_a^2}{4\pi}+\frac{\varepsilon_a}{4\pi}\right]E_t^2\,, \tag{C4}$$

$$b=\frac{m_6k_yk_z(K_{22}-K_{11})-m_2m_8}{m_2m_5-m_1m_6}\,, \tag{C5}$$

$$c=\frac{m_1m_7-m_3m_5}{m_2m_5-m_1m_6}\,, \tag{C6}$$

$$d=\Lambda_3+\Lambda_4E_t^2=\frac{m_1k_yk_z(K_{11}-K_{22})}{m_2m_5-m_1m_6}-\frac{m_5(K_{11}k_z^2+K_{22}k_y^2+K_{33}k_x^2)}{m_2m_5-m_1m_6}+\frac{m_5}{m_2m_5-m_1m_6}\left[\frac{g_7k_x\varepsilon_a^2}{4\pi}+\frac{\varepsilon_a}{4\pi}\right]E_t^2, \tag{C7}$$

$$\frac{1}{T_g}=\frac{m_1m_8+m_5k_yk_z(K_{11}-K_{22})}{m_2m_5-m_1m_6}\,. \tag{C8}$$

The Λ_1, Λ_2, Λ_3, and Λ_4 are defined in (C4) and (C7). In (C3–C8) we use the shorthand

$$m_1=-\gamma_1-\frac{g_1k_yk_z(\gamma_1+\gamma_2)}{2k_xN}+\frac{g_4}{N}\left[\frac{k_x(\gamma_1-\gamma_2)}{2}+\frac{k_z^2(\gamma_1+\gamma_2)}{2k_x}\right], \tag{C9}$$

$$m_2=-\frac{g_2k_yk_z(\gamma_1+\gamma_2)}{2k_xN}+\frac{g_5}{N}\left[\frac{k_x(\gamma_1-\gamma_2)}{2}+\frac{k_z^2(\gamma_1+\gamma_2)}{2k_x}\right], \tag{C10}$$

$$m_3=-\frac{g_3k_yk_z(\gamma_1+\gamma_2)}{2k_xN}+\frac{g_6}{N}\left[\frac{k_x(\gamma_1-\gamma_2)}{2}+\frac{k_z^2(\gamma_1+\gamma_2)}{2k_x}\right]-g_7\varepsilon_a\,, \tag{C11}$$

$$m_5=\frac{g_4k_yk_z(\gamma_1+\gamma_2)}{2k_xN}-\frac{g_1}{N}\left[\frac{k_x(\gamma_1-\gamma_2)}{2}+\frac{k_y^2(\gamma_1+\gamma_2)}{2k_x}\right], \tag{C12}$$

$$m_6=\gamma_1+\frac{g_5k_yk_z(\gamma_1+\gamma_2)}{2k_xN}-\frac{g_2}{N}\left[\frac{k_x(\gamma_1-\gamma_2)}{2}+\frac{k_y^2(\gamma_1+\gamma_2)}{2k_x}\right], \tag{C13}$$

$$m_7=\frac{g_6k_yk_z(\gamma_1+\gamma_2)}{2k_xN}-\frac{g_3}{N}\left[\frac{k_x(\gamma_1-\gamma_2)}{2}+\frac{k_y^2(\gamma_1+\gamma_2)}{2k_x}\right], \tag{C14}$$

$$m_8=-K_{11}k_y^2-K_{22}k_z^2-K_{33}k_x^2\,, \tag{C15}$$

where

$$N=-k_x^5\eta_1^2-k_x^3(k_y^2+k_z^2)\left[\eta_1\frac{\gamma_1+2\alpha_1+3\alpha_4+\beta}{2}\right]-\frac{(k_y^2+k_z^2)^3}{k_x}\left[\eta_2\frac{\alpha_4}{2}\right]-k_x(k_y^2+k_z^2)^2\times\left[\eta_1\eta_2+\alpha_4\frac{\gamma_1+2\alpha_1+2\alpha_4+\beta}{4}\right], \tag{C16}$$

$$g_1=k_x^2k_yk_z\left[\eta_1\frac{\gamma_1+\gamma_2}{2}+\frac{(\gamma_1+2\alpha_1+\alpha_4+\beta)\ (\gamma_2-\gamma_1)}{4}\right]+(k_y^3k_z+k_yk_z^3)\left[\eta_2\frac{\gamma_2-\gamma_1}{2}+\alpha_4\frac{\gamma_1+\gamma_2}{4}\right], \tag{C17}$$

$$g_2=k_x^4\left[\eta_1\frac{\gamma_2-\gamma_1}{2}\right]-k_y^4\left[\alpha_4\frac{\gamma_1+\gamma_2}{4}\right]+k_z^4\left[\eta_2\frac{\gamma_2-\gamma_1}{2}\right]-k_y^2k_z^2\left[\eta_2\frac{\gamma_1-\gamma_2}{2}+\alpha_4\frac{\gamma_1+\gamma_2}{4}\right]-k_y^2k_x^2\left[\eta_1\frac{\gamma_1+\gamma_2}{2}+\alpha_4\frac{\gamma_1-\gamma_2}{4}\right]+k_x^2k_z^2\left[\frac{(\gamma_1+2\alpha_1+2\alpha_4+\beta)\ (\gamma_2-\gamma_1)}{4}\right], \tag{C18}$$

$$g_3=k_xk_yk_z\left[\frac{\gamma_1+2\alpha_1+\alpha_4+\beta}{2}\right]+\frac{k_yk_z(k_y^2+k_z^2)}{k_x}\eta_2, \tag{C19}$$

-

$$g_4=k_x^4\left[\eta_1\frac{\gamma_2-\gamma_1}{2}\right]+k_y^4\left[\eta_2\frac{\gamma_2-\gamma_1}{2}\right]-k_z^4\left[\alpha_4\frac{\gamma_1+\gamma_2}{4}\right]-k_x^2k_z^2\left[\eta_1\frac{\gamma_1+\gamma_2}{2}+\alpha_4\frac{\gamma_1-\gamma_2}{4}\right]+k_y^2k_z^2\left[\eta_2\frac{\gamma_2-\gamma_1}{2}-\alpha_4\frac{\gamma_1+\gamma_2}{4}\right]+k_x^2k_y^2\left[\frac{(\gamma_1+2\alpha_1+2\alpha_4+\beta)\,(\gamma_2-\gamma_1)}{4}\right], \tag{C20}$$

$$g_5=k_x^2k_yk_z\left[\eta_1\frac{\gamma_1+\gamma_2}{2}+\frac{(\gamma_1+2\alpha_1+\alpha_4+\beta)\,(\gamma_2-\gamma_1)}{4}\right]+(k_y^3k_z+k_yk_z^3)\left[\eta_2\frac{\gamma_2-\gamma_1}{2}+\alpha_4\frac{\gamma_1+\gamma_2}{4}\right], \tag{C21}$$

$$g_6=k_x\left[k_x^2\eta_1+k_z^2\frac{\alpha_4}{2}\right]+k_xk_y^2\left[\frac{\gamma_1}{2}+\alpha_1+\alpha_4+\frac{\beta}{2}\right]+\frac{k_y^2(k_y^2+k_z^2)}{k_x}\eta_2\,, \tag{C22}$$

$$g_7=-\frac{k_x}{k_x^2\varepsilon_\parallel+\varepsilon_\perp(k_y^2+k_z^2)}, \tag{C23}$$

$$\eta_1 = \tfrac{1}{2}\left[\alpha_4 - \gamma_2 + \tfrac{1}{2}(\beta + \gamma_1)\right], \tag{C24}$$

$$\eta_2 = \tfrac{1}{2}\left[\alpha_4 + \gamma_2 + \tfrac{1}{2}(\beta + \gamma_1)\right]. \tag{C25}$$

References

1. Kai, S., Kai, T., Takata, M., Hirakawa, K.: J. Phys. Soc. Jpn. **47**, 1379 (1979)
2. Brand, H., Schenzle, A.: J. Phys. Soc. Jpn. **48**, 1382 (1980)
3. Kawakubo, T., Yanagita, A., Kabashima, S.: J. Phys. Soc. Jpn. **50**, 1451 (1981)
4. Brand, H.R., Kai, S., Wakabayashi, S.: Phys. Rev. Lett. **54**, 555 (1985)
5. Kai, S., Fukunaga, H., Brand, H.R.: J. Phys. Soc. Jpn. **56**, 3759 (1987)
6. Kai, S., Fukunaga, H., Brand, H.R.: J. Stat. Phys. **54**, 1133 (1989)
7. Kai, S.: In: Noise in nonlinear dynamical systems. Moss, F., McClintock, P.V.E. (eds.), vol. 3, p. 22. Cambridge: Cambridge University Press 1989; Brand, H.R.: Ibidem p. 77
8. Kai, S., Hirakawa, K.: Prog. Theor. Phys. Supp. **64**, 212 (1978)
9. Ribotta, R., Joets, A., Lei, L.: Phys. Rev. Lett. **56**, 1595 (1986)
10. Kai, S., Chizumi, N., Kohno, M.: Phys. Rev. A **40**, 6554 (1989)
11. Kai, S., Zimmermann, W.: Prog. Theor. Phys. Supp. **99**, 458 (1989)
12. Bodenschatz, E., Zimmermann, W., Kramer, L.: J. Phys. (Paris) **49**, 1875 (1988)
13. Horsthemke, W., Doering, C.R., Lefever, R., Chi, A.S.: Phys. Rev. A **31**, 1123 (1985)
14. Behn, U., Müller, R.: Phys. Lett. A **113**, 85 (1985)
15. Müller, R., Behn, U.: Z. Phys. B **69**, 185 (1987)
16. Müller, R., Behn, U.: Z. Phys. B **78**, 229 (1990)
17. Madhusudana, N.V., Raghunathan, V.A.: Mol. Cryst. Liq. Cryst. Lett. **5**, 201 (1988)
18. Zimmermann, W., Kramer, L.: Phys. Rev. Lett. **55**, 402 (1985)
19. Kramer, L., Bodenschatz, E., Pesch, W., Thom, W., Zimmermann, W.: Liq. Cryst. **5**, 699 (1989)
20. Zimmermann, W.: In: Nematics – Mathematical and Physical Aspects. Coron, J.-M., Ghidaglia, J.-M., Hélein, F. (eds.) p. 401. Dordrecht, Boston, London: Kluwer Academic Publishers 1991
21. Thom, W., Zimmermann, W., Kramer, L.: Liq. Cryst. **4**, 309 (1989)
22. Madhusudana, N.V., Raghunathan, V.A., Sumathy, K.R.: Pramāna J. Phys. **28**, L311 (1987)
23. Raghunathan, V.A., Madhusudana, N.V.: Pramāna J. Phys. **31**, L163 (1988)
24. Raghunathan, V.A., Madhusudana, N.V.: Mol. Cryst. Liq. Cryst. Lett. **6**, 103 (1989)
25. Meyer, R.B.: Phys. Rev. Lett. **22**, 918 (1969)
26. Kelker, H., Hatz, R.: Handbook of Liquid Crystals, p. 203. Weinheim: Chemie Verlag (1980)
27. Delev, V.A., Scaldin, O.A., Chuvyrov, A.N.: Mol. Cryst. Liq. Cryst. **215**, 179 (1992)
28. Delev, V.A., Scaldin, O.A.,Chuvyrov, A.N.: Liq. Cryst. **12**, 441 (1992)
29. Dubois-Violette, E., de Gennes, P.G., Parodi, O.: J. Phys. (Paris) **32**, 305 (1971)
30. Goossens, W.J.A.: In: Advances in liquid crystals. Brown, G.H. (ed.), vol. 3, p. 1. New York, San Francisco, London: Academic Press 1978
31. Maheswara Murthy, P.R., Raghunathan, V.A., Madhusudana, N.V.: Liq. Cryst. **14**, 483 (1993)
32. Madhusudana, N.V., Durand, G.: J. Phys. (Paris) **46**, L-195 (1985). As reasons for the errros were mentioned the screening of the bulk electric field by surface counterions and the possible existence of space charges in the bulk, related to the anisotropy of conductivity. The effect of the latter is estimated by $\sim 15\%$ and is commented by "which is not important in the present stage". Thus we assume for the impact of the screening the same variance of 15% which gives the resulting 30% error
33. Dozov, I., Martinot-Lagarde, Ph., Durand, G.: Phys. Lett. **43**, L-365 (1982)
34. Shapiro, V.E., Loginov, V.M.; Physica A **91**, 563 (1978)
35. Hirata, S., Taco, T.: Jap. J. Appl. Phys. **20**, L459 (1981)
36. Chuvyrov, A.N., Chigrinov, V.G.: Sov. Phys. JETP **60**, 101 (1984)
37. Smith, I.W., Galerne, Y., Lagerwall, S.T., Dubois-Violette, E., Durand, G.: J. Phys. (Paris) **36**, C1-237 (1975)
38. Lange, A.: Thesis, Leipzig (1993)
39. Lefever, R., Horsthemke, W.: In: Nonlinear phenomena in chemical dynamics. Vidal, C., Pacault, A. (eds.), pp 120. Berlin, Heidelberg, New York: Springer 1981
40. Bourett, R.C., Frisch, U., Pouquet, A.: Physica **65**, 303 (1973)
41. Arnold, L., Kloeden, P.: SIAM J. Appl. Math. **49**, 1242 (1989)
42. Behn, U., Lange, A.: Electrohydrodynamic convection in liquid crystals driven by multiplicative noise: sample stability. (to be published)
43. Feigel'mann, M.V., Staroselsky, I.E.: Z. Phys. B **62**, 261 (1986)
44. Behn, U., Schiele, K., Teubel, A.: Wiss. Zeitschrift Karl-Marx-Universität Leipzig. Math.-Naturwiss. R. **34**, 602 (1985); Lippert, K., Schiele, K., Behn, U., Kühnel, A.: In: Nonlinear Coherent Structures in Physics and Biology. Remoissenet, M., Peyrard, M. (eds.), p. 209. Berlin, Heidelberg, New York: Springer 1991